ADVANCES IN ATMOSPHERIC SCIENCES, VOL. 36, JULY 2019, 711–720

• **Original Paper** •

Striping Noise Analysis and Mitigation for Microwave Temperature Sounder-2 Observations

Xiaolei ZOU* and Xiaoxu TIAN

Earth Science System Interdisciplinary Center, University of Maryland, College Park, Maryland 20742*, USA*

(Received 12 January 2019; revised 23 March 2019; accepted 8 April 2019)

ABSTRACT

The Microwave Temperature Sounder (MWTS)-2 has a total of 13 temperature-sounding channels with the capability of observing radiance emissions from near the surface to the stratosphere. Similar to the Advanced Technology Microwave Sounder (ATMS), striping pattern noise, primarily in the cross-track direction, exists in MWTS-2 radiance observations. In this study, an algorithm based on principal component analysis (PCA) combined with ensemble empirical mode decomposition (EEMD) is described and applied to MWTS-2 brightness temperature observations. It is arguably necessary to smooth the first three principal component (PC) coefficients by removing the first four intrinsic mode functions (IMFs) using the EEMD method (denoted as PC3/IMF4). After the PC3/IMF4 noise mitigation, the striping pattern noise is effectively removed from the brightness temperature observations. The noise level in MWTS-2 observations is significantly higher than that detected in ATMS observations. In May 2014, the scanning profile of MWTS-2 was adjusted from varying-speed scanning to constant-speed scanning. The impact on striping noise levels brought on by this scan profile change is also analyzed here. The striping noise in brightness temperature observations worsened after the profile change. Regardless of the scan profile change, the striping noise mitigation method reported in this study can more or less suppress the noise levels in MWTS-2 observations.

Key words: MWTS-2, striping noise, temperature sounding, microwave radiometry

Citation: Zou, X., and X. Tian, 2019: Striping noise analysis and mitigation for Microwave Temperature Sounder-2 observations. *Adv. Atmos. Sci.*, **36**(7), 711–720, https://doi.org/10.1007/s00376-019-9009-x.

Article Highlights:

- MWTS-2 observations are contaminated with striping pattern noise that is greater in magnitude than that of the ATMS.
- The scan profile change implemented on MWTS-2 in May 2014 made striping noise stronger.
- The PCA/EEMD method can effectively mitigate the striping noise in MWTS-2 observations before or after the profile change.

1. Introduction

FengYun (FY)-3C was successfully launched into a sun-synchronous orbit on 23 September 2013. It is the third satellite in the new series of the Chinese FY polar-orbiting fleet. The FY-3 mission aims at enhancing numerical weather prediction and climate research with observations, monitoring large-scale natural disasters, and providing meteorological information for aviation and navigation purposes. The first and second satellites of this series, i.e., FY-3A and FY-3B, were launched into their orbits on 27 May 2008 and 5 November 2010, respectively. The local equator crossing times of FY-3A, -3B, and -3C are 1000, 1400, and 2200, respectively. The Microwave Temperature Sounder (MWTS)-2 is one of the 11 sensors onboard FY-3C. The MWTS-2 contains 13 channels whose central frequencies range from 50.3 GHz to 57.6 GHz corresponding to the Advanced Technology Microwave Sounder (ATMS) channels 3–15. Table 1 lists the central frequencies and peak weighting function pressures of the MWTS-2 channels. As a cross-track microwave radiometer, the MWTS-2 has 90 fields-of-view (FOVs) on each scan line, and the swath width of the MWTS-2 is 2600 km (Tian et al., 2018).

During 12–18 May 2014, the scan profile of the FY-3C MWTS-2 was changed. Before this scan profile change, each scan cycle took 2.67 seconds. The antenna of the MWTS-2 scans at cold space, a warm target, and the earth scene with the same integration time of 0.018 s and accelerates during the time in between. After the profile change, the MWTS-2 kept a constant speed during each entire scan cycle of 5.23 s. MWTS-2 data from 5–11 March 2014 and 29 May to 4 June 2014 are used in this study. There are 14–15 swaths in a single day. Each swath contains around 2400 and 1200 scan

* Corresponding author: Xiaolei ZOU
Email: xzou1@umd.edu

Table 1. Central frequencies of FY-3C MWTS and corresponding ATMS channels.

Channel number		Central frequency (GHz)		Peak weighting function (hPa)	
MWTS	ATMS	MWTS	ATMS	MWTS	ATMS
1	3	50.3		Surface	
2	4	51.76		950	
3	5	52.8		850	
4	6	53.596 ± 0.115		700	
5	7	54.4		400	
6	8	54.94		250	
7	9	55.5		200	
8	10	57.2903		100	
9	11	57.2903 ± 0.115		50	
10	12	57.2903		25	
11	13	57.2903 ± 0.322		10	
12	14	$57.2903 \pm 0.322 \pm 0.010$		5	
13	15	$57.2903 \pm 0.322 \pm 0.004$		2	

lines before and after the scan profile change, respectively.

Numerous previous studies have demonstrated the significance of observations from temperature sounders such as the MWTS-2 and ATMS. Tian and Zou (2016) described an improved temperature retrieval algorithm for temperature sounder observations and applied the results to hurricane cases to analyze three-dimensional warm-core structures. Tian and Zou (2018) examined the temporal evolutions of thermal structures in the 2017 Hurricanes Harvey, Irma, and Maria using retrievals from temperature sounder observations. Zou and Tian (2018) developed a global positioning system radio occultation-based temperature retrieval algorithm with limb-corrected and remapped ATMS observations. As MWTS-2 has similar channel configurations, these recently proposed temperature retrieval algorithms are all readily applicable to MWTS-2 observations. There was a significant reduction in the random noise level in the results. Temperature sounder observations have also been shown to have positive impacts on hurricane track and intensity forecasts (Zou et al., 2013; Li et al., 2016; Li and Liu, 2016) as well as on global weather forecast skills (Eyre et al., 1993; Andersson et al., 1994; Derber and Wu, 1998). Tian et al. (2018) showed that MWTS-2 observations, after limb correction, could be used to monitor tropical cyclones. The nonrandom, striping pattern noise found in ATMS observations may possibly be due to the 1/f noise in its receiver (Bormann et al., 2013; Qin et al., 2013). Li et al. (2016) reported slightly higher analysis and forecast errors when assimilating MWTS-2 observations due to the striping noise. Zou et al. (2017) described a principal component analysis (PCA) combined with Ensemble Empirical Mode Decomposition (EEMD) striping noise mitigation method for ATMS that is applicable to all temperature-sounding channels as well as window channels. Striping issues have also been found in the predecessors of MWTS-2, the MWTS onboard FY-3B, as well as the ATMS onboard the recently launched National Oceanic and Atmospheric Administration (NOAA-20) satellite (Li and Zou, 2015; Zou and Tian, 2019).

In this study, the PCA/EEMD striping noise mitigation is adopted and applied to MWTS-2 observations before and after the scan profile change to analyze the MWTS-2 striping noise characteristics. The same mitigation method can be readily applicable to other instruments, including the previous MWTS on previous FY-3 satellite series.

2. Striping noise mitigation algorithm

The data matrix composed of MWTS-2 brightness temperatures can be expressed as

$$\boldsymbol{A}_{M\times N} = \begin{pmatrix} y_{1,1} & \cdots & y_{N,1} \\ \vdots & \ddots & \vdots \\ y_{1,M} & \cdots & y_{N,M} \end{pmatrix}, \tag{1}$$

where $y_{k,i}$ is the brightness temperature at FOV position i of the kth scan line. In this study, each data sample consists of 200 scan lines. M denotes the total number of FOVs in one scan line. In the case of MWTS-2, this is equal to 90. N is the total number of scan lines in the analysis sample. The matrix $\boldsymbol{A}_{M\times N}$ can be decomposed into $M = 90$ PC modes,

$$\boldsymbol{A} = \sum_{j=1}^{90} \boldsymbol{e}_j \boldsymbol{u}_j^{\mathrm{T}}, \tag{2}$$

where the jth mode is the product of the PC coefficient $\boldsymbol{u}_j$ and the PC component $\boldsymbol{e}_j$. The PC coefficient describes along-track features while the PC component is a function of the FOV position (Qin et al., 2013; Zou et al., 2017). For each individual observation pixel, Eq. (2) can also be written as

$$y_{k,i} = \sum_{j=1}^{90} e_{j,i} u_{k,j}. \tag{3}$$

An EEMD method (Wu and Huang, 2009) can then be employed to remove the striping noise in the decomposed MWTS-2 observations, i.e., $y_{k,i}$. The smoothed brightness temperature, $\bar{y}_{\mathrm{EEMD},k,i}$, can then be calculated by removing the first three intrinsic mode functions (IMFs) of the first PC, $u_{k,1}$, as follows:

$$\bar{y}_{\mathrm{EEMD},k,i} = e_{1,i}\left(u_{i,1} - \sum_{m=1}^{3} \mathrm{IMF}_m(k)\right) + \sum_{j=2}^{90} e_{j,i} u_{k,j}. \tag{4}$$

The EEMD-smoothed PC coefficient can then be expressed as $u_{\mathrm{EEMD},k,1} = u_{k,1} - \sum_{m=1}^{L} \mathrm{IMF}_m(k)$, where L denotes the number of IMFs to be removed.

The spectra for the first six IMFs of the first four PC coefficients at channel 8 for 1 May 2014 are shown in Fig. 1. Peak magnitudes of the first four IMFs are at the frequencies greater than 10^{-2} Hz. The amplitude of an individual IMF decreases with PC coefficient sequence, i.e., all IMFs have the largest amplitudes for the first PC coefficient and the smallest amplitudes for the fourth PC coefficient. This is in accordance with the fact that the first PC component explains the majority of variances. The peak magnitudes of the IMFs

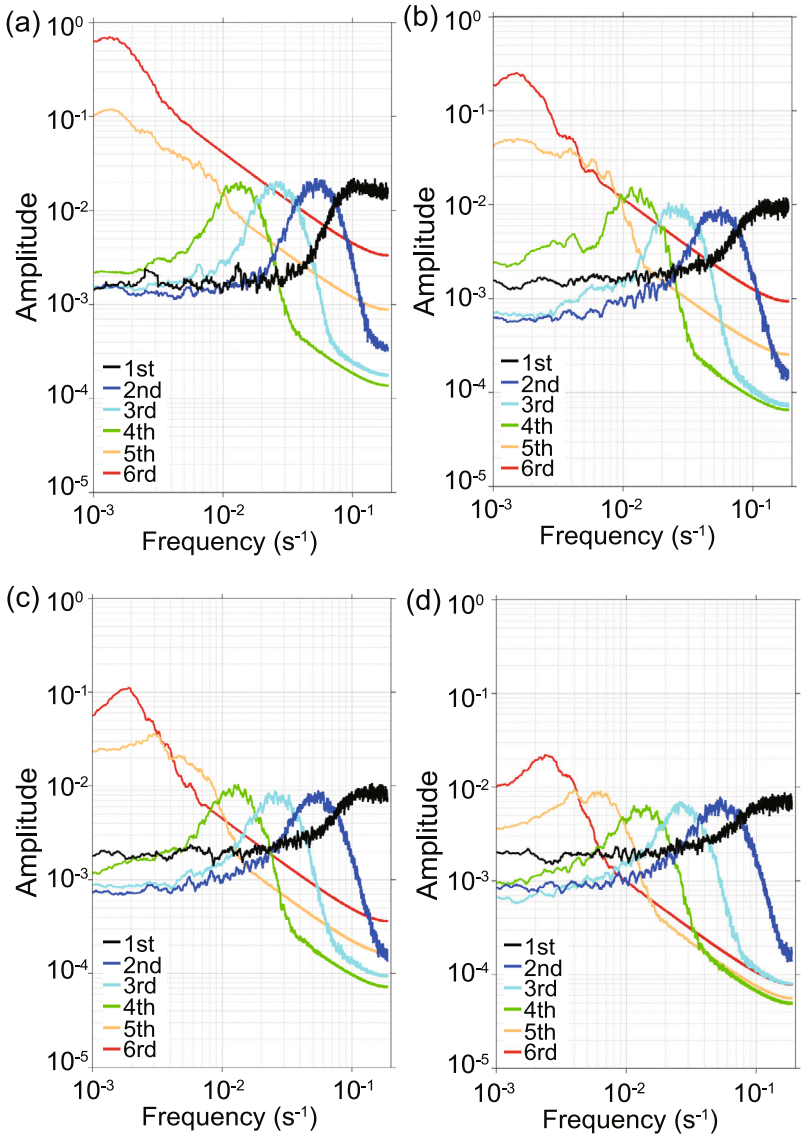

Fig. 1. Fourier spectra for the first six IMFs of the (a) first, (b) second, (c) third, and (d) fourth PC coefficients at channel 8 for MWTS-2 observations on 1 May 2014.

of the first three PC coefficients start to increase noticeably after the fourth IMF. For example, the peak magnitudes of the fifth IMFs are ~10 times greater than the peak magnitudes of the first four IMFs. The absolute majority of the variances in observations from signals such as weather signals, instrument scan patterns, as well as striping noise are accounted for by the first three principal components (Qin et al., 2013; Zou et al., 2014). For the fourth PC coefficient, there is no clear difference in the peak magnitudes of the six IMFs. We thus choose to remove the first four IMFs of the first three PC coefficients, denoted as PC3/IMF4 for brevity. The distribution of the first five PC modes (i.e., eigenvectors) for the 47th MWTS-2 data sample (k = 47, each sample includes 200 scan lines) on 1 May 2014 is displayed in Fig. 2. Note that the eigenvectors are functions of FOV positions. All PC modes oscillate around zero, and their values are close in scale. Compared with other PC modes, the first PC mode

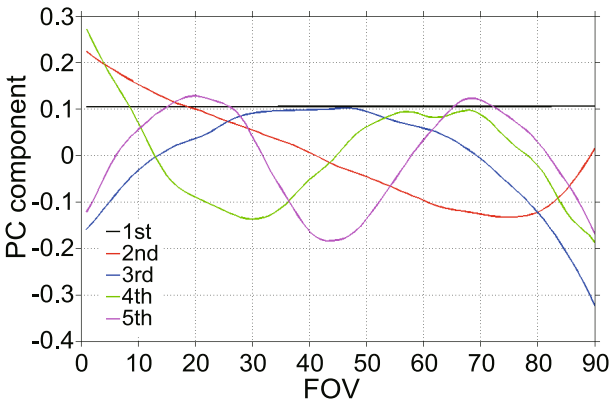

Fig. 2. Spatial distributions of the first five PC modes (i.e., eigenvectors) for the 47th MWTS-2 data sample (k = 47, each sample includes 200 scan lines) on 1 May 2014.

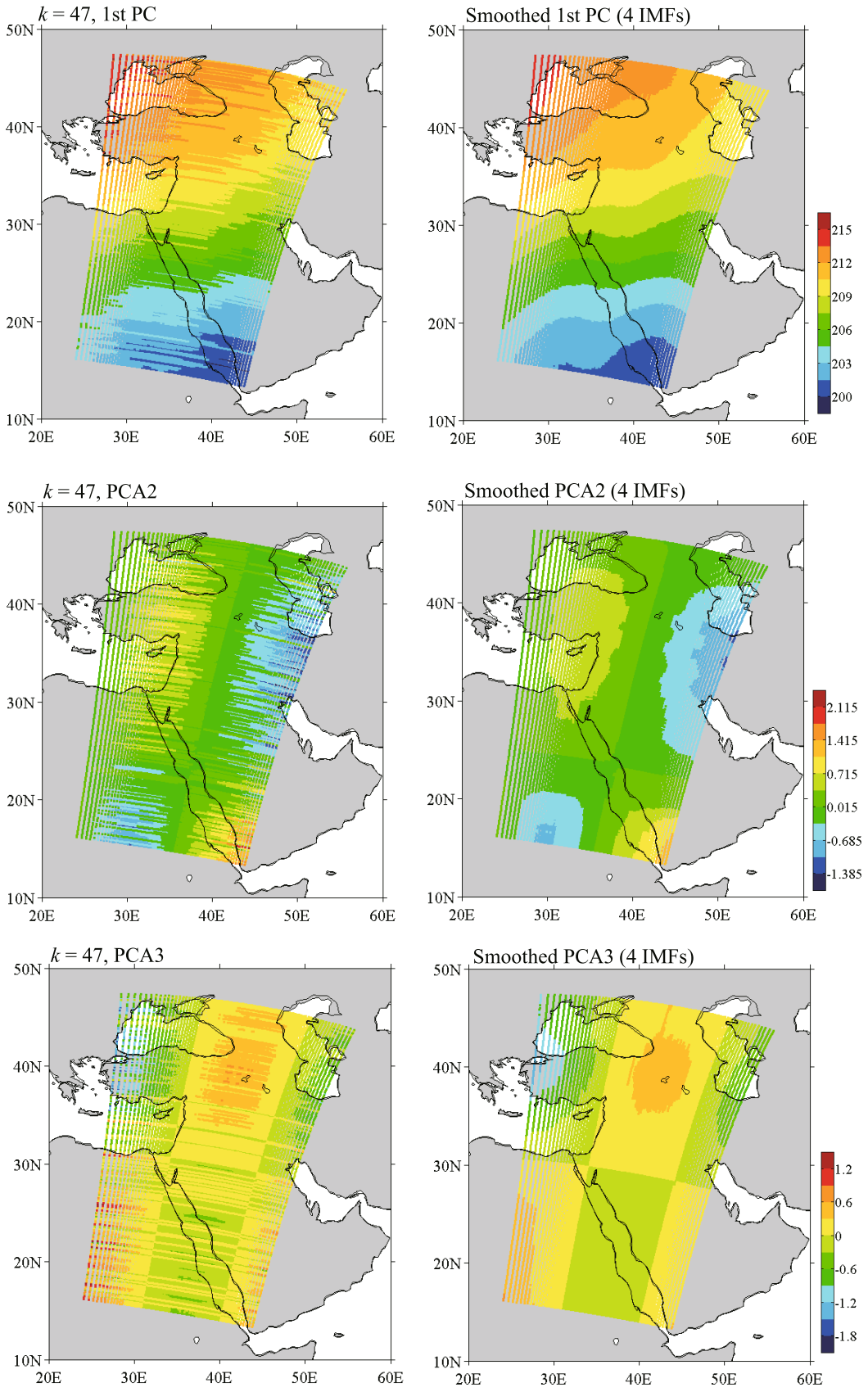

Fig. 3. Spatial distributions of the first three PCA components (i.e., the product of an eigenvalue and an eigenvector) before (left panels) and after (right panels) striping noise mitigation for the 47th data sample ($k = 47$, each sample includes 200 scan lines) on 1 May 2014.

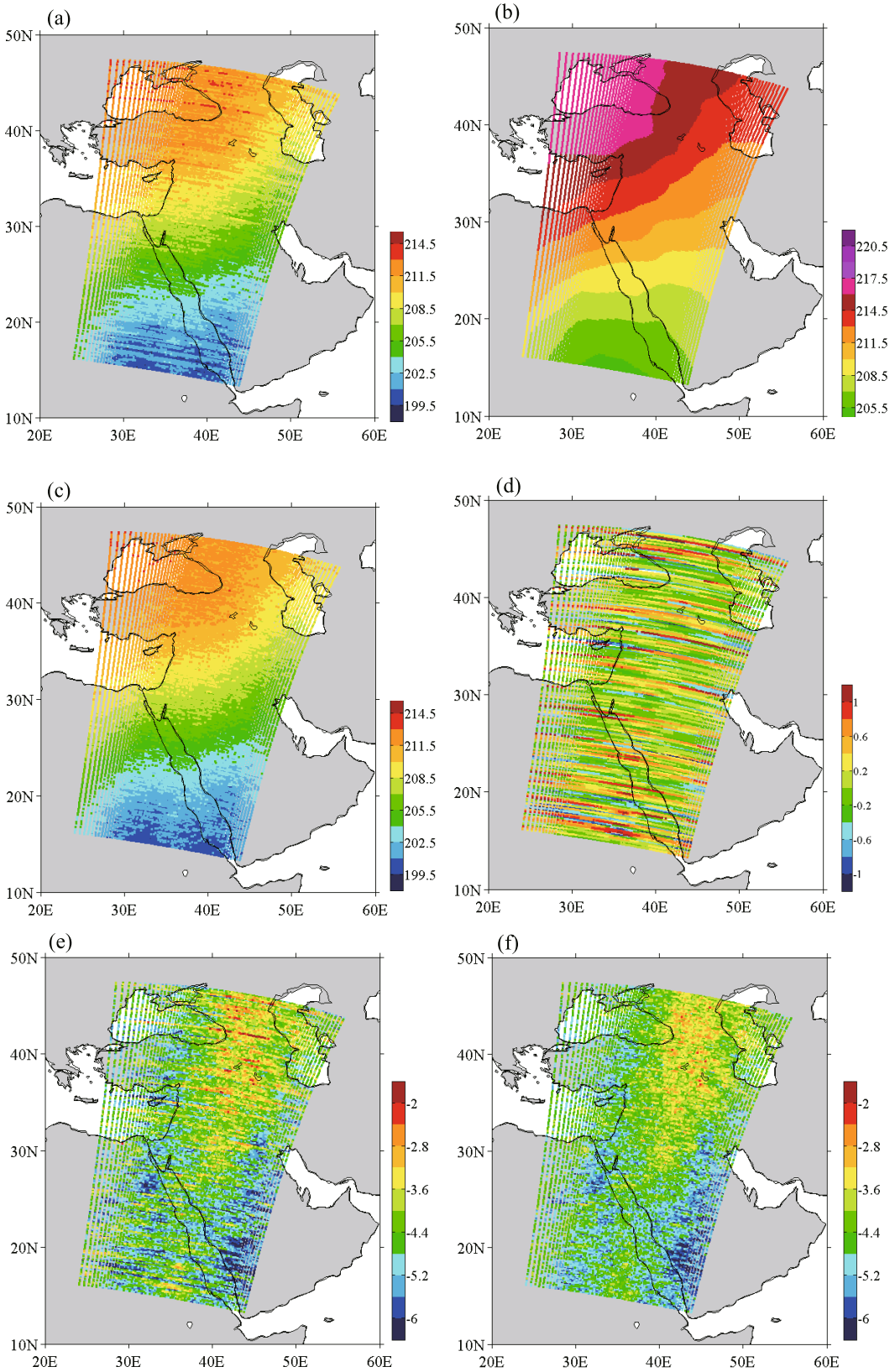

Fig. 4. Spatial distributions of MWTS-2 channel 8 (a) observed, (b) simulated, and (c) smoothed brightness temperatures (units: K) for the 47th data sample ($k = 47$, each sample includes 200 scan lines) on 1 May 2014. The first four IMFs of the first three PC coefficients are removed in (c). (d) Differences between (a) and (c). (e) Differences between (a) and (b). (f) Differences between (c) and (b).

changes little. This is reasonable because the first PC mode represents the major cross-track scan features of the MWTS-2 while the other PC modes capture weather signals. The numbers of extrema for the second, third, fourth, and fifth PC modes are two, three, four, and five, respectively. Figure 3 shows the spatial distributions of the first, second, and third PC components, i.e., the products of PC coefficients and the corresponding PC modes. The magnitude of the first PC component is the greatest, comparable in magnitude to the brightness temperature. The second and third PC components have magnitudes of the same order. The PC components before and after smoothing are calculated as the PC coefficients with and without the first four IMFs removed, respectively. Before the noise mitigation, visible striping noise exists in all the three PC components. After smoothing, the striping noise is removed while large-scale features in the along-track and cross-track directions remain unchanged.

The Community Radiative Transfer Model is used in this study to simulate MWTS-2 brightness temperatures using the 6-h forecast field generated from the National Centers for Environmental Prediction Global Forecast System as the background. This was done to bring out the striping noise in observed brightness temperatures. The spatial distributions of the observed (O) and simulated (B) brightness temperatures on 1 May 2014 are displayed in Figs. 4a and b. The striping noise can be easily identified from the observed brightness temperature field. Figure 4c shows the spatial distribution after the PC3/IMF4 striping noise mitigation. Compared with Fig. 4a, no striping noise is found in the distribution of PC3/IMF4-smoothed brightness temperatures. The spatial distributions of the differences between observations and simulations ($O-B$) before and after the PC3/IMF4 noise mitigation are shown in Figs. 4e and f, respectively. The striping noise pattern clearly seen in Fig. 4e is effectively removed after PC3/IMF4 smoothing. Figure 5 shows the global distributions of ($O-B$) before and after the PC3/IMF4 striping noise mitigation on 1 May. It is clear that after smoothing, the visible striping noise is effectively removed while other

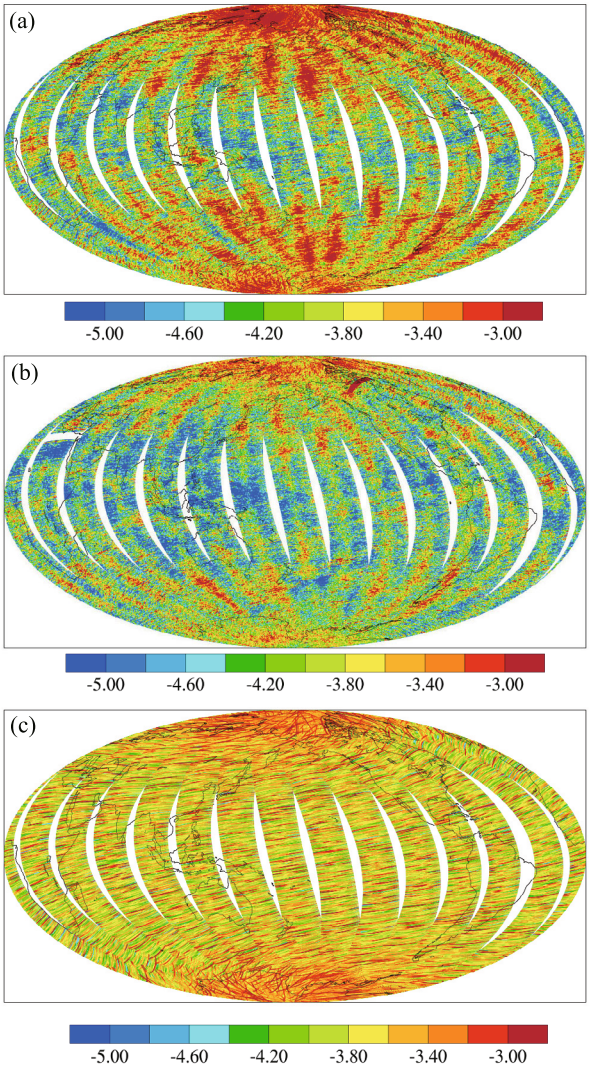

Fig. 5. Global distributions of channel 8 (a) $O-B$ and (b) differences between smoothed brightness temperatures removed on 1 May 2014 on the ascending node. The first four IMFs of the first three PC coefficients are removed for noise mitigation. (c) The removed striping noise. Units: K.

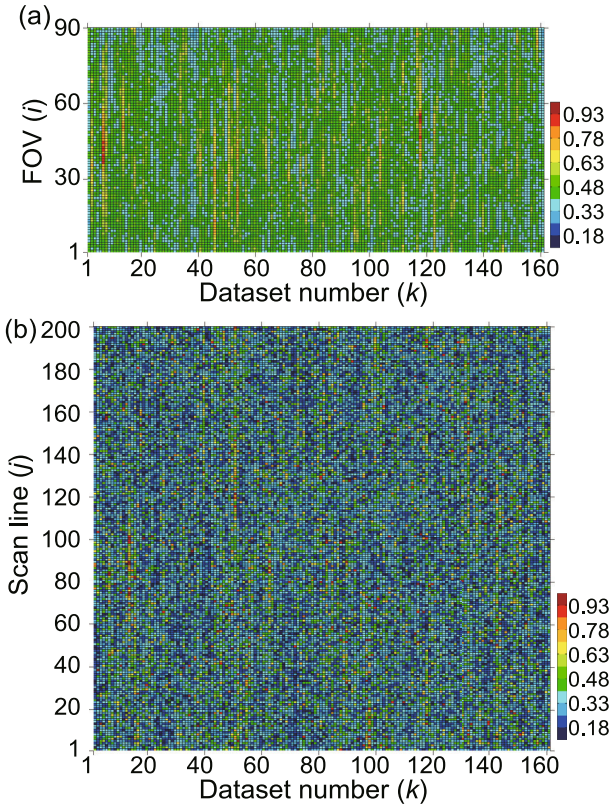

Fig. 6. Variations in (a) along-track variances for channel 8 as a function of the sample group number and FOV (i) and (b) cross-track variances as a function of dataset number (k) and scan line (j) before striping noise mitigation on 1 May 2014. The total number of scan lines in each dataset is 200. The total number of datasets for both the ascending and descending nodes on 1 May is 162.

weather-related features are not altered. The noise removed is shown in Fig. 5c.

3. Striping index calculated for FY-3C MWTS-2 global data

To quantitatively validate the effectiveness of the striping noise mitigation on FY-3C MWTS observations, a striping index as a measure of uniform accuracy for brightness temperature is defined here. The Striping Index (SI) for a single day at a given channel is calculated as

$$\mathrm{SI} = \frac{\sum_{k=1}^{K} \frac{1}{N} \sum_{i=1}^{N} \sigma^2_{\mathrm{along}}(k,i)}{\sum_{k=1}^{K} \frac{1}{M} \sum_{j=1}^{M} \sigma^2_{\mathrm{cross}}(k,j)} , \tag{5}$$

where $\sigma^2_{\mathrm{along}}(k,i)$ and $\sigma^2_{\mathrm{cross}}(k,j)$ are along-track and across-track variances, respectively. The variances are calculated as follows:

$$\begin{aligned} \sigma^2_{\mathrm{along}}(k,i) &= \frac{1}{M} \sum_{j=1}^{M} ((O-B)_{k,i,j} - \overline{(O-B)}_{k,i,j})^2 , \\ \overline{(O-B)}_{k,i,j} &= \frac{1}{M} \sum_{j=1}^{M} (O-B)_{k,i,j} , \end{aligned} \tag{6}$$

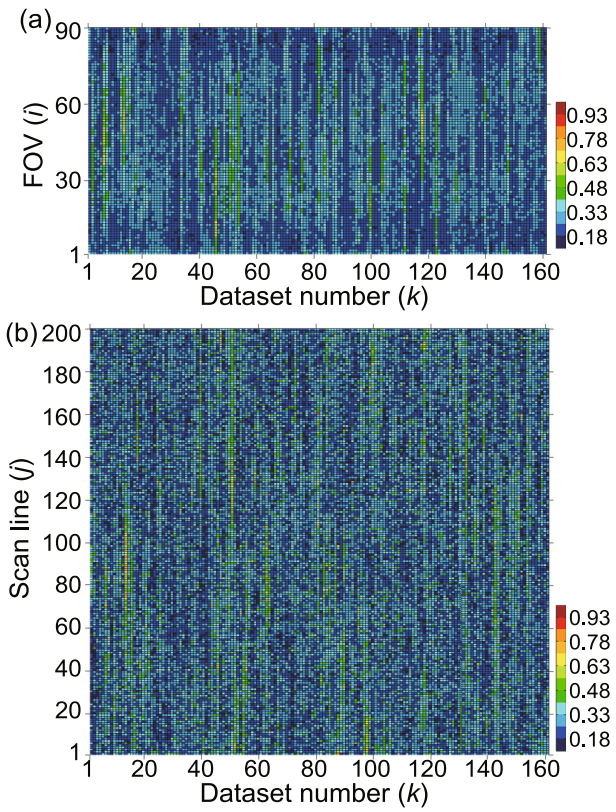

Fig. 7. As in Fig. 6 except for data with striping noise mitigated (PC3/IMF4). The mean value of the striping index at channel 8 is 0.975.

$$\begin{aligned} \sigma^2_{\mathrm{cross}}(k,j) &= \frac{1}{N} \sum_{i=1}^{N} ((O-B)_{k,i,j} - \overline{(O-B)}_{k,i,j})^2 , \\ \overline{(O-B)}_{k,i,j} &= \frac{1}{N} \sum_{i=1}^{N} (O-B)_{k,i,j} , \end{aligned} \tag{7}$$

where $(O-B)_{k,i,j}$ stands for the $(O-B)$ difference at the ith FOV on the jth scan line within the kth data sample, N is the total number of FOVs, M is the number of scan lines within each of the datasets for the variance calculation, and K is the total number of data samples. In the calculation, $N = 90$, $M = 200$, and K is around 160. The smoothed brightness temperatures will be denoted as O_{smooth} for SIs after noise mitigation.

Figure 6 shows the variations in along-track variances $\sigma^2_{\mathrm{along}}(k,i)$ and cross-track variances $\sigma^2_{\mathrm{cross}}(k,j)$ calculated using brightness temperatures before striping noise mitigation

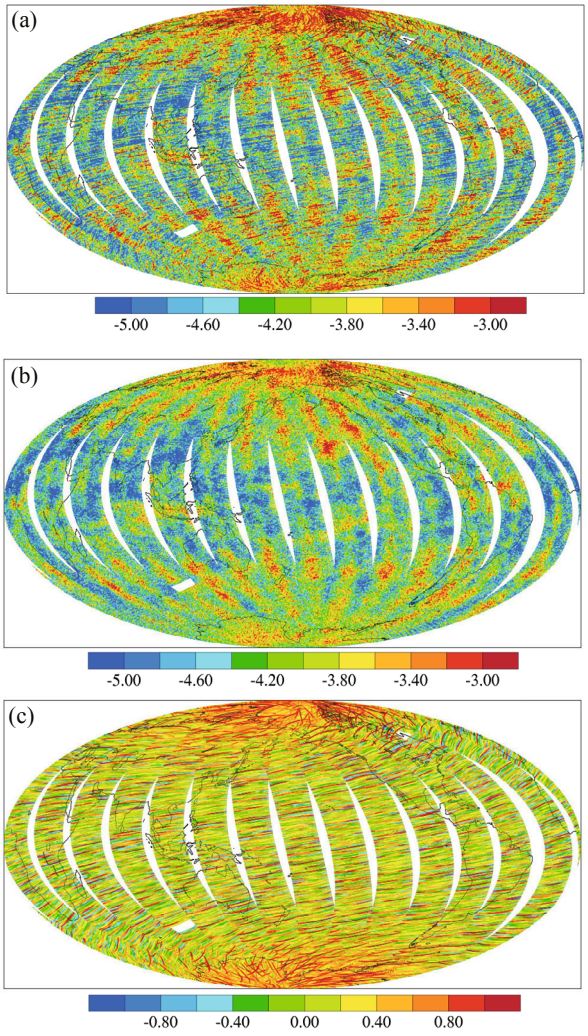

Fig. 8. Global distributions of channel 8 (a) $O-B$ and (b) differences between smoothed brightness temperatures removed on 30 May 2014 on the ascending node. The first three IMFs of the first three PC coefficients are removed for noise mitigation. (c) The removed striping noise. Units: K.

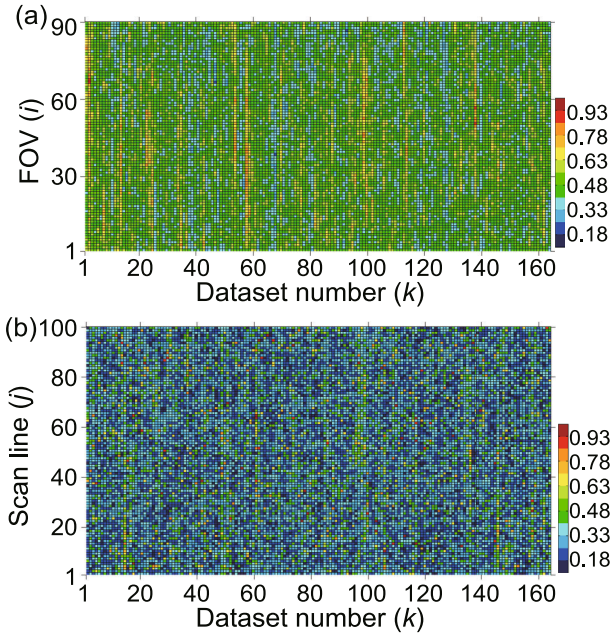

Fig. 9. Variations in (a) along-track variances as a function of the sample group number and FOV (i) and (b) cross-track variances as a function of dataset number (k) and scan line (j) before striping noise mitigation on 30 May 2014. The total number of scan lines in each dataset is 100. The total number of datasets for both the ascending and descending nodes on 30 May is 164. (c) Variations in striping index as a function of dataset number (k). The dashed line shows the mean striping index (equal to 1.5146).

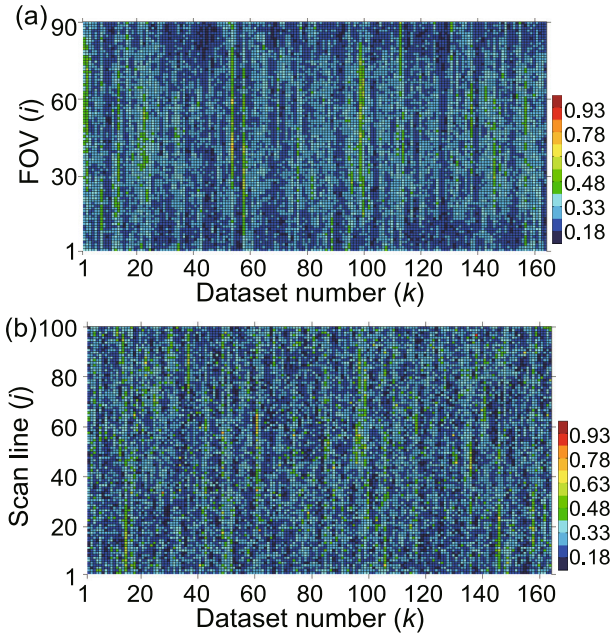

Fig. 10. As in Fig. 9 except for data with striping noise mitigated (3PC/3IMF). The mean value of the striping index is 1.013.

on 1 May 2014. The distribution of the along-track variance has line patterns for adjacent FOVs within some data samples due to cross-track correlations. By comparison, the distribution of the cross-track variance appears to be more random. The along-track variances generally have larger values than the cross-track variances, confirming that striping noise adds to along-track variances. The striping index calculated using Eq. (5) for Fig. 6 is 1.3513. Figure 7 shows variations in along-track variances $\sigma^2_{\text{along}}(k,i)$ and cross-track variances $\sigma^2_{\text{cross}}(k,j)$ after striping noise mitigation. The magnitudes of the along-track variances are significantly reduced while those of the cross-track variances change very little. The striping index for Fig. 7 is now reduced to 0.975.

4. Impact of profile change on striping noise

During the period 12–18 May, a scan profile change was implemented on the MWTS-2 instrument, prior to which it took 2.67 s to finish one scan cycle. Since the scan profile change, the MWTS-2 scans at a constant pace of 5.23 s per scan cycle. The striping noise results from 29 May to 4 June 2014 are shown to illustrate the influence of the scan profile change. Similar to Fig. 5, Fig. 8 shows the global distributions of $(O-B)$ before and after striping noise mitigation on 30 May 2014. After the scan profile change, the striping noise in MWTS-2 observations is similar in magnitude as those before the scan profile change (Fig. 5). The along-track and cross-track variances of the observations on 30 May 2014 before and after destriping are shown in Figs. 9 and 10, respectively. Comparing the results in Fig. 9 with those in Fig. 6 (1 May), the along-track variances are visibly greater, while no significant increase can be seen in the cross-track variances. The SI for MWTS-2 observations after the scan profile change increased from 1.35 (Fig. 6) to 1.51 (Fig. 9). After destriping, the SI in Fig. 10 drops to 1.01, which is still high compared with the destriped observations before the scan profile change (0.98 in Fig. 7).

Figure 11 shows the variations in SIs of MWTS-2 channel 8 with respect to date during two one-week periods. Along-track variances increased after the scan profile change while cross-track variances remained about the same, suggesting that the FY-3C MWTS-2 striping problem became even more severe after the scan profile change. The along-track variations after striping noise mitigation were noticeably reduced. The cross-track variations also decreased slightly due to the smoothing within the second and third PC coefficients. The SI index hovers around 1.0 after noise mitigation, indicating the effectiveness of the noise mitigation reported in this study.

5. Summary and conclusions

Striping pattern noise in the along-track direction exists in MWTS-2 observations. In this study, the PCA/EEMD method described by Zou et al. (2017) is applied to MWTS-2 brightness temperature observations to detect and mitigate the striping noise. Striping noise exists in not only the first PC coefficient but also in the second and third PC coefficients.

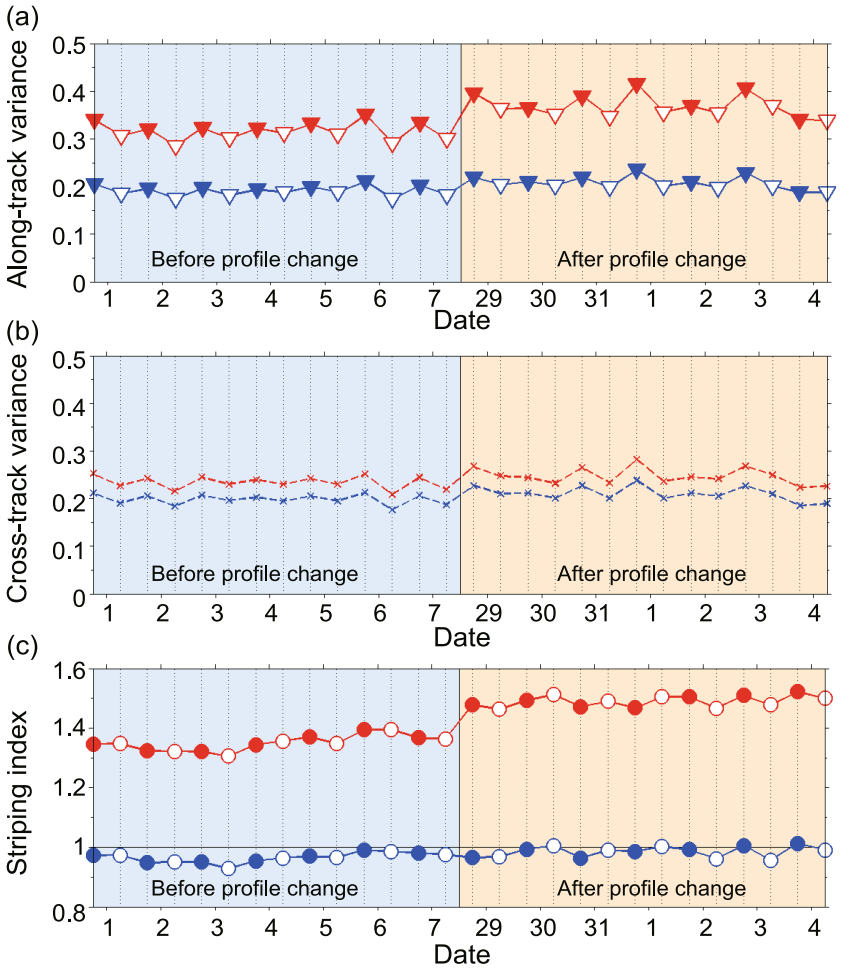

Fig. 11. (a) Along-track variances, (b) cross-track variances, and (c) striping index at channel 8 during 1–7 May 2014 and 29 May to 4 June 2014 before (red) and after (blue) noise mitigation. Ascending and descending nodes are shown as open and solid markers, respectively.

The magnitude of the striping noise in the temperature-sounding channels can be as great as 1 K, which is much greater than the noise level in ATMS observations (Qin et al., 2013). For the purpose of a quantitative analysis, a global striping index is defined based on the variances of brightness temperature observations in both along-track and cross-track directions. This index shows that, because of the existing striping noise, the along-track variance is significantly larger than the variance in the cross-track direction. After noise mitigation, the global striping index decreased dramatically to a value of one, suggesting the effectiveness of the noise mitigation algorithm reported in this study. During 12–18 May 2014, a scan profile change was implemented. After the scan profile change, the antenna on the MWTS-2 started to rotate at a constant pace. Striping noise in the observations for a two-week period after the scan profile change reveals that the noise level became even higher after the profile change. From another perspective, this suggests that the root cause of the striping noise in microwave sensors does not lie in the scanning pace.

Acknowledgements. This research was supported by the National Key R&D Program (Grant No. 2018YFC1506702). The authors thank the FengYun Satellite Data Center (http://satellite.nsmc.org.cn) for providing the MWTS-2 observations. The authors also thank Dr. Yuan MA for conducting some of this work during her Ph.D. studies and the anonymous reviewers for their time and contributions to this study. The software developed to perform the calculations in this study is available by contacting the corresponding author at xzou1@umd.edu.

REFERENCES

Andersson, E., J. Pailleux, J.-N. Thépaut, J. R. Eyre, A. P. McNally, G. A. Kelly, and P. Courtier, 1994: Use of cloud-cleared radiances in three/four-dimensional variational data assimilation. *Quart. J. Roy. Meteor. Soc.*, **120**, 627–653, https://doi.org/10.1002/qj.49712051707.

Bormann, N., A. Fouilloux, and W. Bell, 2013: Evaluation and assimilation of ATMS data in the ECMWF system. *J. Geophys. Res.*, **118**, 12 970–12 980, https://doi.org/10.1002/2013JD020325.

Derber, J. C., and W.-S. Wu, 1998: The use of TOVS cloud-cleared radiances in the NCEP SSI analysis system. *Mon. Wea. Rev.*, **126**, 2287–2299, https://doi.org/10.1175/1520-0493(1998)126<2287:TUOTCC>2.0.CO;2.

Eyre, J. R., G. A. Kelly, A. P. McNally, E. Andersson, and A. Persson, 1993: Assimilation of TOVS radiance information through one-dimensional variational analysis. *Quart. J. Roy. Meteor. Soc.*, **119**, 1427–1463, https://doi.org/10.1002/qj.49711951411.

Li, J., and X. L. Zou, 2015: Assimilation of FY-3 MWTS radiance data into Chinese NWP systems. World Climate Research Programme, section 1, pp 11–15.

Li, J., and G. Q. Liu, 2016: Assimilation of Chinese Fengyun-3B Microwave Temperature Sounder radiances into the global GRAPES system with an improved cloud detection threshold. *Frontiers of Earth Science*, **10**, 145–158, https://doi.org/10.1007/s11707-015-0499-2.

Li, J., G. Q. Liu, J. Li, and G. Q. Liu, 2016: Direct assimilation of Chinese FY-3C Microwave Temperature Sounder-2 radiances in the global GRAPES system. *Atmospheric Measurement Techniques*, **9**, 3095–3113, https://doi.org/10.5194/amt-9-3095-2016.

Qin, Z. K., X. L. Zou, and F. Z. Weng, 2013: Analysis of ATMS striping noise from its Earth scene observations. *J. Geophys. Res.*, **118**, 13 214–13 229, https://doi.org/10.1002/2013JD020399.

Tian, X. X., and X. L. Zou, 2016: ATMS- and AMSU-A-derived hurricane warm core structures using a modified retrieval algorithm. *J. Geophys. Res.*, **121**, 12 630–12 646, https://doi.org/10.1002/2016JD025042.

Tian, X. X., and X. L. Zou, 2018: Capturing size and intensity changes of hurricanes Irma and Maria (2017) from polar-orbiting satellite microwave radiometers. *J. Atmos. Sci*., **75**, 2509–2522, https://doi.org/10.1175/JAS-D-17-0315.1.

Tian, X. X., X. L. Zou, and S. P. Yang, 2018: A limb correction method for the Microwave Temperature Sounder 2 and its applications. *Adv. Atmos. Sci*., **35**, 1547–1552, https://doi.org/10.1007/s00376-018-8092-8.

Wu, Z. H., and N. E. Huang, 2009: Ensemble empirical mode decomposition: A noise-assisted data analysis method. *Advances in Adaptive Data Analysis*, **1**, 1–41, https://doi.org/10.1142/S1793536909000047.

Zou, X., F. Weng, B. Zhang, L. Lin, Z. Qin, and V. Tallapragada, 2013: Impacts of assimilation of ATMS data in HWRF on track and intensity forecasts of 2012 four landfall hurricanes. *J. Geophys. Res.*, **118**, 11 558-11 576, https://doi.org/10.1002/2013JD020405.

Zou, X., H. Dong, and Z. Qin, 2017: Striping noise reduction for ATMS window channels using a modified destriping algorithm. *Quart. J. Roy. Meteor. Soc.*, **143**, 2567–2577, https://doi.org/10.1002/qj.3107.

Zou, X. L., and X. X. Tian, 2018: Hurricane warm-core retrievals from AMSU-A and remapped ATMS measurements with rain contamination eliminated. *J. Geophys. Res.*, **123**, 10 815–10 829, https://doi.org/10.1029/2018JD028934.

Zou, X. L., and X. X. Tian, 2019: Comparison of ATMS striping noise between NOAA-20 and S-NPP and noise impact on warm core retrieval of typhoon jelawat (2018). *IEEE Journal of Selected Topics in Applied Earth Observations and Remote Sensing*, 1–9, https://doi.org/10.1109/JSTARS.2019.2891683. (in press)

Zou, X. L., X. X. Tian, and F. Z. Weng, 2014: Detection of television frequency interference with satellite microwave imager observations over oceans. *J. Atmos. Oceanic Technol.*, **31**, 2759–2776, https://doi.org/10.1175/JTECH-D-14-00086.1.